

DESY SR 83-20
November 1983

Eigentum der Property of	DESY	Bibliothek library
Zugang: Accessions:	2 0. DEZ. 1983	
Leihfrist: Loan period:	7	Tage days

EXTRINSIC PHOTOCONDUCTIVITY IN XENON-DOPED FLUID ARGON AND KRYPTON

by

R. Reiniger, I.T. Steinberger

Racah Institute of Physics, The Hebrew Univ., Jerusalem

S. Bernstorff

II. Institut für Experimentalphysik, Universität Hamburg

V. Saile

Hamburger Synchrotronstrahlungslabor HASYLAB at DESY

P. Laporte

Equipe de Spectroscopie C.N.R.S. (LA 171), Saint Etienne

ISSN 0723-7979

NOTKESTRASSE 85 · 2 HAMBURG 52

DESY behält sich alle Rechte für den Fall der Schutzrechtserteilung und für die wirtschaftliche Verwertung der in diesem Bericht enthaltenen Informationen vor.

DESY reserves all rights for commercial use of information included in this report, especially in case of filing application for or grant of patents.

To be sure that your preprints are promptly included in the
HIGH ENERGY PHYSICS INDEX ,
send them to the following address (if possible by air mail) :

DESY
Bibliothek
Notkestrasse 85
2 Hamburg 52
Germany

Extrinsic photoconductivity in xenon-doped
fluid argon and krypton.

R. Reininger^{a*}, S. Bernstorff^b, P. Laporte^d,
V. Saile^c and I.T. Steinberger^a

^a Racah Institute of Physics, The Hebrew University, Jerusalem, Israel

^b II. Inst. für Experimentalphysik, Universität Hamburg, 2000 Hamburg 50,
Germany

^c HASYLAB, Deutsches Elektronen-Synchrotron DESY, Notkestr. 85, 2000 Ham-
burg 52, Germany

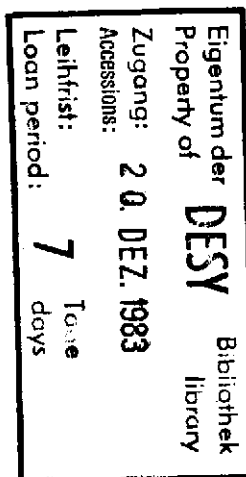
^d Equipe de Spectroscopie C.N.R.S. (LA 171), 158 bis cours Fauriel,
42023 Saint Etienne, Cedex, France

Abstract

Monochromated synchrotron radiation from the DORIS storage ring at DESY was used to excite photoconduction in xenon-doped fluid argon for densities ranging from 0.7 to $2.1 \times 10^{22} \text{ cm}^{-3}$, in xenon-doped fluid krypton from 1.3 to $1.6 \times 10^{22} \text{ cm}^{-3}$ as well as in solid Xe/Ar. The measurements yielded directly the ionization energy E_G^i of the impurity in the dense medium. Using previous experimental results on the energy V_0 of the conduction electron in conjunction with E_G^i the polarization energy P_+^i of a hole trapped at a xenon atom was also determined for the respective density ranges. These experimental P_+^i values differ considerably from theoretical predictions. Combining the E_G^i values with results from absorption spectra by Messing et al. led to the determination of the binding energy and effective mass of the Wannier-Mott impurity exciton and indicated that previous assignments of absorption bands in xenon-doped solid argon have to be revised.

* Present address: HASYLAB, Deutsches Elektronen-Synchrotron DESY, 2000 Ham-
burg 52, Germany

Submitted to Chem. Phys.



1. Introduction

There exists a wealth of experimental results on the energy levels of excitons trapped by various atomic impurities in rare-gas solids. The experimental methods employed include vacuum ultraviolet absorption [1-5], luminescence excitation [4,6,7] and photoemission spectroscopy [4,8-10]. These studies led, among other results, to the determination of the energy levels of the trapped exciton, as well as its ionization energy, binding energy, and effective mass. In the corresponding liquids, however, our knowledge of these data is incomplete for two reasons: a) no photoemission measurements have been performed on these liquids that would yield the position of the ground state of the impurity; b) in rare-gas liquids (doped [3,4,11-14] or pure [15-17]) at most the $n=1$ and $n=2$ Wannier exciton levels could be observed, the higher levels being smeared out or submerged in the tail of the conduction band. These two levels are insufficient for the determination of the binding energy and the effective mass since for the $n=1$ exciton the Wannier scheme cannot be applied without corrections [18,19].

Doped rare-gas fluids were subject to intensive studies concerning perturbations by the host on atomic Rydberg states of the impurity and the evolution of the perturbation effects with increasing density [12-14]. The line shapes and shifts were analysed in terms of the semiclassical statistical theory and yielded information on excited state potentials [12,14]. These studies also led to an experimental criterion distinguishing between the $n=2$ Wannier exciton trapped at the impurity atom and perturbed atomic levels [13].

Reflection spectra of pure fluid xenon revealed that certain bands appearing in the spectrum are due to free excitons; these excitons were shown to be entities different from perturbed atomic levels. The evolution of the exciton bands with increasing fluid density were followed in detail [20,21]. One of the results was the definition of the minimum conditions

necessary for the appearance of the excitons [21]. The energetic positions of each exciton in the liquid was found to be in good correspondence with those in the solid, if the density change involved in the phase transition was taken into account [17]. Photoconductivity excitation spectra in xenon have furnished the width E_G of the forbidden gap as well as the dependence of E_G on the thermodynamic conditions from the gas to the triple-point liquid [22,23] and to the solid [24]. These results have completed the characterization of excitons obtained from reflection spectroscopy [16,17,20,21] under a wide range of conditions. Moreover in conjunction with direct measurements of the energy V_G of the conduction electron [25,26], the results served to obtain a detailed description of the evolution of the conduction and valence bands in the fluid [23,27].

For pure krypton, the photoconductivity threshold was observed only for a limited range of thermodynamic conditions [28] since optical excitations shift towards shorter wavelengths with decreasing atomic number and the cutoff of LiF normally sets an upper photon energy threshold to the measurements. For the same reason photoconduction in fluid argon and neon could not be studied hitherto.

It is demonstrated in this work that even with the limitations of a LiF window one can obtain useful photoconductivity results on the lighter rare gases provided doped samples are used. The investigations yielded directly the energy E_G^i needed to transfer an electron from a xenon impurity level to the conduction levels of the host (argon or krypton) under various thermodynamic conditions. Coupling the E_G^i -values with absorption spectra results [13] on the $n=2$ Wannier-Mott exciton led to the determination of the binding energies of the trapped excitons and their effective masses. Moreover, from the values of E_G^i and those of the energy V_G of the quasi-free electron [25,26] it was possible to give, for the first time, experimental values of the polarization energy P_+^i and to compare them with theory. The

results of this work led to a critical discussion of previous assignments of electronic excitations in doped rare gas solids.

2. Experimental details

The experiments were performed using synchrotron radiation from the DORIS storage ring at DESY monochromated by means of the HONORMI system [29]. The sample cell was different from that used in previous studies [23,25]: the "miniconflat" construction was preserved but the electrode system consisted now of two metal platelets parallel to the incident beam having a length of 1 cm with a distance of 2 mm between them. This arrangement ensured efficient electron collection in spite of the rather weak absorption due to the low concentration of the impurity atoms. The simple geometry permitted calculating the electric field from the applied voltage and the interelectrode distance. The gas mixture was prepared at room temperature in a bakeable gas-handling system after this had been pumped down to 10^{-5} Pa (10^{-10} bar). The mixture was then collected at 77°K in a cold finger next to the cell. This followed transferring most of the mixture to the experimental cell by warming the finger and cooling the cell. During these operations as well as during the actual experiments the pressure in the system was kept well above (by the order of 10^6 Pa) the saturated vapour pressure of the liquid in the cell. Such a procedure was reported to favour thorough mixing of the constituents of the sample and prevent aggregate formation [3]. For the Xe/Ar system nominal xenon concentrations of 1.6, 20, 30 and 200 ppm were employed; for Xe/Kr we used only a nominal impurity concentration of 10 ppm. Possible enrichment of the mixture upon cooling was not checked, but the positions of the energy levels found in Xe/Ar were independent of the xenon concentration within the above range and therefore any eventual enrichment was immaterial for the results. The density range of the argon fluid was varied between 0.15 to $2.05 \times 10^{22} \text{ cm}^{-3}$, the temperature

from 299 down to 94°K and the pressure from 10^6 to 7×10^7 Pa. For krypton, the density range was 1.3 to $1.8 \times 10^{22} \text{ cm}^{-3}$ corresponding to temperatures from 180 to 113°K and pressures from 1.2 to 3.5×10^6 Pa*.

3. Results

a. Xe:Ar

Figure 1 presents photoconductivity excitation spectra for four host densities. The spectra are normalized for equal numbers of photons arriving at the LiF window of the cell. Graph d is for the solid and the others for three different fluid densities. In all spectra one can observe a clear photoconductivity threshold, a maximum and a decrease to zero at higher photon energies. In the solid there is also a secondary maximum at about 11.65 eV. The broad valley between the two maxima coincides in position with a broad and compound peak in the absorption spectrum [1,2] of solid Xe/Ar. The decrease of the photoresponse to zero on the blue side of the peak in all spectra can be attributed to the competing $n=1$ $\Gamma(3/2)$ exciton absorption band in the argon host. In the reflection spectrum of pure fluid argon this band is observable [30] starting from a density of $0.63 \times 10^{22} \text{ cm}^{-3}$ and above. Its peak for this density is at 11.55 eV, shifting towards the blue (like the high photon energy edge of the photoconductivity peak in Fig. 1) with increasing density; for $n=2.1 \times 10^{22} \text{ cm}^{-3}$ this excitonic reflection peak is at 11.78 eV and for the triple-point solid at 11.93 eV. Since this band is due to very strong absorption in the host the penetration depth of the light even at its long-wavelength tail is much smaller than that determined by the dilute impurity. In fact, the light will be absorbed in a thin layer (of the order of 100 nm or less) of the fluid adjacent to the window. Even if the energy of some of the host excitons is consequently transferred to an impurity [8] and this were to release electrons into the conduction band, the lifetime of the electrons created near the window would be very low resulting in negligible photocurrent.

* The critical parameters for Ar are: $n_c = 0.811 \times 10^{22} \text{ cm}^{-3}$, $T_c = 150.9^\circ \text{K}$ and $p_c = 4.8 \times 10^6$ Pa; for Kr $n_c = 0.66 \times 10^{22} \text{ cm}^{-3}$, $T_c = 209.4^\circ \text{K}$ and $p_c = 5.4 \times 10^6$ Pa

The overall consistency of the results was checked by repeating some of the curves of Fig. 1 with different voltages applied. The electric field, as calculated from the geometry, was varied from 50 to 2000 volt/cm. It was found that if the photocurrents were divided by the appropriate value of the (field-dependent) electron mobility as determined by Huang and Freeman [3] the resulting curves were congruent within the experimental error. This showed that the photocurrents measured were proportional to μn_o , μ being the electron mobility at the density and voltage given and n_o the concentration of conduction electrons. The threshold for impurity photoconduction E_{pc}^i was determined by two empirical methods: a) plotting all graphs on such scales that they should be roughly congruent in the threshold region (while shifted along the photon energy scale) and then noting the photon energy at which the current starts to rise; b) plotting the square root of the current as a function of the photon energy and extrapolating the linear part of this plot to find its intercept with the photon energy axis. The first method furnished results systematically higher than the second one, the maximum difference being 0.07 eV. We note that in pure xenon [23] there was no such systematic difference between the two sets of results.

Figure 2 is based on averages of pairs of results taken from the two sets, showing the dependence of the threshold energy on argon density for the various xenon concentrations mentioned above. It is clear from the figure that within the set limits the xenon concentration is irrelevant to the position of the threshold; mention was made of this fact already above. It should be borne in mind that a photoconductivity threshold can be perceived even at densities below those presented in Figs. 1 and 2, namely down to $n=0.7 \times 10^{22} \text{ cm}^{-3}$, but because of the smallness of the signal when compared with the background noise it was not possible to establish the threshold photon energy for such low densities with an acceptable accuracy (see, e.g., Fig. 1a).

Figure 2 shows that E_{pc}^i is practically constant from $n=1.75 \times 10^{22} \text{ cm}^{-3}$ to the highest argon densities, but it rises somewhat (by about 0.08 eV) at lower densities. The value of E_{pc}^i in solid xenon-doped argon is slightly higher than that in the triple-point liquid. For comparison, the value of E_G^i in the solid, as determined from Wannier exciton series by Baldini [1,2] at about 8°K is also shown. The value obtained by Baldini is lower by about 0.4 eV than that determined in this work. The difference between the two results cannot be attributed to the different temperatures of measurement, since E_{pc}^i should decrease (though only slightly) with increasing temperature [17] instead of decreasing.

One may write $E_{pc}^i = E_G^i + E_G^i$, being the energetic distance between the ground level of the impurity within the host and the lowest conduction level. Doing so the eventual existence of localized states at the lower edge of the conduction band is neglected; the high values of the zero-field mobility of the electrons [31] and the relatively steep rise of the photocurrent at the threshold justify this assumption. E_G^i , in turn, is related to the ionization potential I_G^i of the xenon atom (12.13 eV), the polarization energy P_+^i of the positive xenon core and the energy V_0 of the conduction electron in argon by means of the following equation [3]

$$E_G^i = I_G^i + V_0 + P_+^i \quad \dots \quad 1$$

V_0 for argon has been measured [26] throughout the whole range of thermodynamic conditions covered this work. The values P_+^i determined from Eq. 1 appear in Fig. 3. The figure also includes calculated values of the adiabatic electrostatic potential energy as given by Messing and Jortner [32]. These authors used a self-consistent screening function to calculate the electrostatic interaction between the ion and its surroundings, taking into account the pair correlation functions between the impurity ion and

the host atoms and between host atom pairs. It is seen in the figure that the values calculated by Messing and Jortner [32] are higher (by 0.33 eV at the triple-point) than those determined in this work. The results of another, simplified calculation also appear in Fig. 3: we used the Born charging energy formula

$$P_+^i = \frac{e^2}{2\sigma} \left(1 - \frac{1}{\epsilon}\right) \quad \dots \quad 2$$

σ being an effective hard-core radius and ϵ the dielectric constant (taken here to be equal to the square of the refractive index measured at 546.1 nm). In order to get agreement with experiment at the triple point $\sigma = 0.238$ nm was substituted in Eq. 2. ϵ was obtained from Sinnock's work [33] for the dense liquid and the solid; at other densities it was calculated from its value in the triple-point liquid using the Clausius-Mossotti formula. It is seen in Fig. 3 that this calculation yields a $P_+^i(n)$ curve that is considerably steeper than the experimental one; this feature is in common with the results of the sophisticated calculations Messing and Jortner [32].

Figure 4 shows more photocurrent excitation spectra but presented now in such a manner as to emphasize currents observed below the photoconduction threshold. The small currents in this region are probably due to photoinjection into the fluid from one of the metal electrodes. The magnitude of these currents should then be dependent on the exact alignment; this indeed was found to be the case. Another, less likely, explanation for these currents could be extrinsic photoconduction due to some unidentified impurity. It is suggested that in any case the minima of the currents are related to atomic absorption lines of the impurity atom perturbed by molecular effects; if the currents are due to photoinjection, the absorption prevents the light from reaching the electrode and if they are due to photoconduction by means of an unknown impurity, the absorption at the xenon impurity

competes with the absorption that leads to photoconduction. The positions of the current minima and those of the absorption peaks in the Xe/Ar system [13] are compared in Fig. 5. The correspondence between the two sets of data is evident, though only the stronger absorption lines appeared in the present measurements. We note that the photocurrent minimum at around 10.8 eV was not seen in the absorption spectra but the absorption spectra were taken with a MgF₂ window [12] and thus this spectral range was not accessible. The 10.8 eV transition has probably developed from the 6d [0 1/2]₁^o and 6d [1/2]₁^o atomic levels, though no data seem to exist in the literature about these lines for the relevant argon densities.

b. Xe/Kr

In Fig. 6, photoconductivity excitation spectra are shown, normalized for equal numbers of photons transmitted by the LiF window. It was indeed essential to take into account expressly in this case the spectral transmission of the window since important parts of the spectra pertain to the immediate vicinity of the LiF cutoff. It is immediately apparent that the spectra are much noisier than the corresponding ones for Xe/Ar (Fig. 1), indicating, in fact, the smallness of the signal. The reason for this lies in the very high absorption of pure krypton in the region of interest. It has been shown [28] that for densities similar to those of Fig. 6 the reflection spectrum of a pure Kr/MgF₂ interface has one peak around 10 eV and a second one around 10.7 eV: these are the n=1 Γ(3/2) and n'=1 Γ(1/2) excitons respectively. The reflectivity increases by more than a factor of two in the density range of Fig. 6 and the bands also broaden. The shapes of the absorption bands associated with these high reflectances (up to 70 % for the n=1 Γ(3/2) band) could not be evaluated by Kramers-Kronig analysis because of the nearness of the MgF₂ cutoff. Inspection of Fig. 2 in [28] will reveal that because of the strong absorption at the bands discussed radiation will be able to penetrate to the depth of the cell only at three

spectral regions: I. below about 9.5 eV; II. between about 10.3 and 10.6 eV; III. above 10.9 eV. The extensions of these regions become smaller with increasing density. Returning to Fig. 6 it is seen that photocurrent may appear in all three regions. In region I the current is probably due to photoinjection from one of the electrodes or perhaps to photoconduction due to some unknown impurity of the host (cf. the comments on Fig. 4 above). In region II, one observes a sharp peak at about 10.5 eV for the two lower densities. This can be attributed to photoconductivity excited by transitions from the localized xenon levels into the conducting levels of krypton. The drop in response on the high-energy side is caused by the tail of the strong absorption of the 10.7 eV krypton band competing for the photons. On the low energy side, however, it is not sure that the threshold seen (at 10.46 and 10.5 eV respectively in a) and b) can be indeed identified with E_{pc}ⁱ in Xe/Kr: it is possible that the true position of E_{pc}ⁱ is somewhat lower, but it is masked by the tail of the band at 10.0 eV. The total disappearance of the photoconductivity peak in Fig. 6c seems to be due to the broadening of the 10.7 eV krypton band and its increase in height.

Finally in region III two processes can be discerned. At the lower limit of the region xenon impurity photoconduction is seen, generated by photons having larger than the minimum energy E_{pc}ⁱ needed for this process, while the further increase of the current at about 11.5 eV is in the region of the threshold for intrinsic photoconduction [28] of the krypton host. The intrinsic photocurrents are rather small in the present experiments, since due to the very strong absorption all quasi-free electrons are created very near to the LiF window where their lifetime is low.

4. Discussion

The values of E_{pc}^i that were obtained for the Xe/Ar system vary little (0.08 eV) with density in the range investigated. In contrast, for pure Xe in the same range there is a change in the photoconductivity band gap E_{pc} by 0.8 eV [23]. This difference can be conveniently discussed by considering Eq. 1 and the corresponding equation for intrinsic photoconduction:

$$E_{pc} = E_G = I_G + V_o + P^+ + E_v \quad \dots \quad 3$$

All quantities are related now to the pure material, with meanings like in Eq. 1. E_v would be the energy of the top of the "valence band", compared with the ground state of the atom, if a Hartree-Fock type calculation were made not taking into account the essentially many-body effects expressed by the polarization term P^+ . In the density region discussed V_o increases while both P^+ and P_+^i decrease with increasing density. In the case of Xe:Ar the contributions by V_o and P_+^i almost compensate each other, however, in the case of pure xenon the decrease of P^+ with increasing density, seems to be the dominant factor determining the behaviour of E_{pc} .

The availability of spectroscopic results [13] for Xe/Ar for a wide range of densities enables one to calculate several parameters concerning excitons trapped on xenon impurities as well as some characteristics of the host conduction band. Applying, for simplicity, the effective mass theory we write

$$E_n^i = E_G^i - \frac{B^i}{n} \quad n=1,2,3 \quad \dots \quad 4$$

The values of E_G^i given in the present work together with values of E_2^i by Messing et al. [13] yield B^i directly. Substituting $n=1$ in Eq. 4 and comparing the result with the experimental value $E_{|exp}^i$ furnishes the central

cell correction $\Delta E_c = E_1^i - E_{|exp}^i$. Furthermore, writing $B^i = 13.7 \cdot m^*/e^2$ (in electron volts) with values of the optical dielectric constant taken directly from Sinnock [33] or calculated by means of the Clausius-Mossotti formula one gets the effective reduced mass m^* of the exciton (in terms of the free electron mass); since we are dealing with trapped excitons, this is equal to the effective mass of the electrons. Values of $B^i, \Delta E_c$ and m^* thus determined along with the splitting $\Delta_1 = E_1' - E_1$, E_1' being the energy of the $n'=1 \Gamma(1/2)$ exciton and E_1 that of the $n=1 \Gamma(3/2)$ exciton appear in Table 1 for three fluid densities. The corresponding parameters for the solid are also given. It should be noted that all these parameters were obtained directly, without any simplifying assumptions that had to be made in the past because of lack of sufficient experimental data [13,34]. B^i is seen to decrease with increasing density. This decrease is due to the variation of the dielectric constant with density, since the effective mass turns out to be practically constant, 0.55. The central cell correction ΔE_c and the splitting Δ_1 both decrease with density.

Comparison with results of other experiments will be made in two parts. First, we shall deal with results that are not dependent on the tentative assignments made in the past [1-3,13] for the excitonic spectra of solid Xe/Ar; this will be followed by dealing with the assignments.

a) It should be pointed out that the values of the exciton binding energy B^i , the effective mass m^* , and, to a somewhat worse approximation P_+^i , should pertain to pure argon as well: B^i and m^* refer to large-radius excitons, and thus are little influenced by the hole residing on a host atom or on an impurity atom. In P_+^i the nature of the hole should be felt mainly on the contribution of the nearest-neighbour atoms. It is seen in Table 1 that if results on fluid Xe/Ar with solid Ar are compared, both P_+^i and B^i decrease upon the liquid-solid phase transition. Such a decrease could be expected qualitatively on the basis of the increased density and larger dielectric

constant [33] of the solid. However, this does not account for the whole change in B^i ; we note that there is also a decrease by about 15 % in the effective mass upon solidification. The corresponding transition in pure xenon [24] involves an increase of m^* by 10 %. It is not clear, why is the change in opposite directions in the two cases.

The overall consistency of the results of this work with results on pure solid argon as manifested in Table 1 supports directly the spectral assignment by Messing et al. [13] in fluid Xe/Ar. It also demonstrates the effectiveness of the combination of photoconductivity and absorption spectroscopy methods. The results also show two points of discrepancy between theory and experiment: one refers to the P_+^i -values (Fig. 3) and the second to the effective masses [35] (especially in the fluid, Table 1).

b) We turn now to comparisons based on the spectral assignment of the exciton bands in solid Xe/Ar. Table 1 shows that our result for E_{pc}^i is higher by about 0.4 eV than spectroscopic results [1-3,13]. This marked discrepancy seems to be due to erroneous assignment of the $n=2 \Gamma(3/2)$ level in the works quoted. The following arguments support this claim:

1. Pudewill et al. [5] measured absorption spectra for pure neon and for neon doped with argon, krypton and xenon. These authors clearly showed that in Baldini's tentative assignment [1,2] the $n'=1 \Gamma(1/2)$ exciton and the $n=2 \Gamma(3/2)$ exciton had been interchanged. Comparing the Xe/Ne and the Xe/Ar spectra show [1,2] their high degree of likeness; it seems more than plausible that a similar interchange was made in the Xe/Ar case as well.

2. Studying Fig. 5 that summarizes the development of absorption bands [13] in Xe/Ar shows that (assuming Baldini's [1,2] tentative assignment) upon the phase change the $n'=1 \Gamma(1/2)$ and the $n=2 \Gamma(3/2)$ bands interchange their respective positions. No convincing arguments have been brought forward to explain such a situation. Moreover, the study of pure xenon below and above the phase transition [17] did not indicate any "crossover" of this kind.

3. The splitting Δ_1 of the disturbed atomic lines $6s[1/2]_1^0$ and $6s'[0/2]_1^0$ as well as of the related exciton bands $n=1 \Gamma(3/2)$ and $n'=1 \Gamma(1/2)$ decreases monotonically from 1.13 eV to 0.96 eV with the increase of argon density [13] (see Table 1) but "jumps" again (according to the above assignment) to 1.31 eV upon solidification (Table 1). In the Xe/Ne case [13] there is no such discontinuity, Δ_1 decreases with increasing density, including the solid. It is however unexpected, that for both hosts Δ_1 is considerably smaller than the spin-orbit splitting (1.3 eV) of the $5p^6$ levels and of the valence bands in pure Xe

4. Baldini's results [1,2] involve many bands, several of them unassigned. The very high level of doping used in his measurements (1.5 %) may involve dimer formation and correspondingly new levels [36], making the tentative assignments [1,2] rather doubtful.

The above points strongly favour a re-assignment of the absorption spectrum of solid argon doped by xenon. It is suggested that the band observed at 9.97 eV in solid Xe/Ar should be attributed to the $n'=1 \Gamma(1/2)$ exciton and that at 10.53 eV to the $n=2 \Gamma(3/2)$ exciton, i.e., interchanging the current tentative assignments of these bands. Such a re-assignment eliminates all the difficulties enumerated above, though B^i and m^* are smaller than the corresponding quantities for pure solid argon.

A somewhat less direct comparison of the present results with experiment can be made considering the photoemission threshold $E_{Th}^i = E_G^i - V_o$. E_{Th}^i for solid Xe/Ar was determined directly: photoelectron yield spectra [8] furnished $E_{Th}^i = 10.2$ eV and photoelectron distribution curves 10.4 eV [9]. The second method is regarded to be more reliable since it is not influenced by absorption levels competing with the photoemission process. By comparing Wannier exciton series limits and the photoemission threshold in pure solid argon it was found [37] that $V_o = +0.3$ eV. From this $E_G^i = E_{Th}^i + V_o = 10.4 + 0.3 = 10.7$ eV. The agreement with the present result $E_G^i = 10.97$ eV is satisfactory, taking into account the inaccuracies in the determination of E_{Th}^i and V_o .

Because of the experimental difficulties caused by the nearness of host bands to the impurity bands the results for Xe/Kr are much less detailed than for Xe/Ar. Still, one may compare the values of E_{pc}^i and P_+^i in Xe/Kr with corresponding values in Xe/Ar. The results in Xe/Kr are consistently lower than in Xe/Ar for all three quantities, as it could be expected from the larger atomic weight and consequently higher polarizability of krypton. Even so, it should be mentioned that if one combines the result for E_{pc}^i (10.5 eV) in liquid Xe/Kr with the result by Raz and Jortner for the $n=2$ $\Gamma(3/2)$ exciton in the liquid (9.6 eV), $B^i = 3.6$ eV is obtained. This is somewhat larger than B^i in the Xe/Ar system, though it should be smaller. Moreover, it is more than twice larger than B (1.53 eV) in pure solid krypton [38]. These discrepancies are much too big to be attributable to changes in the dielectric constant and the effective mass upon the phase transition.

4. Conclusions

This first study of photoconductivity excitation spectra in doped rare gas fluids and solids demonstrates that electrons can be brought into the quasi-free conduction levels of these very wide gap materials by photoexcitation from impurity levels. Though the impurity centres probably cause a decrease in the lifetime of the photoelectrons, the currents obtained are still conveniently measurable if an appropriate sample cell and synchrotron radiation are used. The technique has been put to use for the determination of the ground state energy of the impurity within the host and, in combination with other measurements, of a series of derived parameters. The first determination of the hole polarization energy P_+^i , based directly on experiment, should be particularly noted. It seems that essentially the same technique could be used for the determination of energy levels and related parameters in many doped wide-gap fluid or solid systems. Moreover, the technique may have also significance in assessing the expected performance of particle detectors based on dense rare gases, since this is the only way to study

single-photon photoconduction in materials having band gaps larger than the LiF cutoff and since impurities may have direct effects on electron mobilities and lifetimes.

5. Acknowledgement

The authors thank HASYLAB and DESY for their support of the project and Dr. U. Asaf for helping in the development of the cell. R.R. and I.T.S. acknowledge the partial support of the Fund for Basic Research, administered by the Israel Academy of Sciences and Humanities.

References

1. G. Baldini and R.S. Knox, Phys. Rev. Lett 11 (1963) 127
2. G. Baldini, Phys. Rev. 137 (1965) 508
3. B. Raz and J. Jortner, Proc. Roy. Soc. London, A317 (1970) 113
4. J. Jortner in Vacuum Ultraviolet Radiation Physics, eds. E.E.Koch, R. Haensel and C. Kunz, (Pergamon Vieweg, London/Braunschweig, 1974) p. 263
5. D. Pudewill, F.J. Himpfel, V. Saile, N. Schwentner, M. Skibowski and E.E. Koch, Phys. Stat. Sol. b74 (1976) 485
6. U. Hahn and N. Schwentner, Chem. Phys. 48 (1980) 53
7. U. Hahn, R. Haensel and N. Schwentner, Phys. Stat. Sol. b109 (1982) 233
8. Z. Ophir, B. Raz, J. Jortner, V. Saile, N. Schwentner, E.E. Koch, M. Skibowski and W. Steinmann, J. Chem. Phys. 62 (1975) 650
9. N. Schwentner and E.E. Koch, Phys. Rev. B14 (1976) 4687
10. R. Nürnberger, F.J. Himpfel, E.E. Koch and N. Schwentner, Phys. Stat. Sol. b81 (1977) 503
11. B. Raz and J. Jortner, Chem. Phys. Lett. 4 (1970) 511
12. I. Messing, B. Raz and J. Jortner, J. Chem. Phys. 66 (1977) 2239
13. I. Messing, B. Raz and J. Jortner, Chem. Phys. 23 (1977) 23
14. I. Messing, B. Raz and J. Jortner, J. Chem. Phys. 66 (1977) 4577
15. D. Beaglehole, Phys. Rev. Lett. 15 (1965) 551
16. U. Asaf and I.T. Steinberger, Phys. Letters A34 (1971) 207
17. I.T. Steinberger and U. Asaf, Phys. Rev. B8 (1973) 914
18. J. Hermanson and J.C. Phillips, Phys. Rev. 150 (1966) 652
19. J. Hermanson, Phys. Rev. 150 (1966) 660
20. P. Laporte and I.T. Steinberger, Phys. Rev. A15 (1977) 2538
21. P. Laporte, J.L. Subtil, U. Asaf, I.T. Steinberger and S. Wind, Phys. Rev. Lett. 45 (1980) 2138
22. R. Reininger, U. Asaf, I.T. Steinberger and P. Laporte, J. Electrostatics 12 (1982) 123

23. R. Reininger, U. Asaf, I.T. Steinberger, V. Saile and P. Laporte, Phys. Rev. B, in press
24. U. Asaf and I.T. Steinberger, Phys. Rev. B10 (1974) 4464
25. R. Reininger, U. Asaf and I.T. Steinberger, Chem. Phys. Lett. 90 (1982) 287
26. R. Reininger, U. Asaf, I.T. Steinberger and S. Basak, Phys. Rev. B, in press
27. R. Reininger, U. Asaf, I.T. Steinberger, P. Laporte, S. Bernstorff and V. Saile, Annals of the Israel Physical Society 6 (1983) 282
28. R. Reininger, U. Asaf, I.T. Steinberger, P. Laporte and V. Saile, Phys. Rev. B26 (1982) 6294
29. V. Saile, P. Gürtler, E.E. Koch, A. Kozevnikov, M. Skibowski and W. Steinmann, Appl. Opt. 15 (1976) 2559
30. S. Bernstorff, P. Laporte, R. Reininger, V. Saile, I.T. Steinberger and J.L. Subtil, Annals of the Israel Physical Society 6 (1983) 270
31. S.S.S. Huang and G.R. Freeman, Phys. Rev. A24 (1981) 714
32. I. Messing and J. Jortner, J. Chem. Phys. 24 (1977) 183
33. A.C. Sinnock, J. Phys. C13 (1980) 2375
34. U. Asaf and I.T. Steinberger, in Extended Abstracts, Fifth International Conference on VUV Radiation Physics, Vol. 1, eds. M.C. Castex, M. Pouey and N. Pouey, publ. "V.U.V.5", C.N.R.S. Meudon, 1977, p. 205
35. J.H. Jahnke, N.A.W. Holzwarth and S.A. Rice, Phys. Rev. A5 (1972) 463
36. T. Nanba, N. Nagasawa and M. Ueta, J. Phys. Soc. Japan 37 (1974) 1031
37. N. Schwentner, M. Skibowski and W. Steinmann, Phys. Rev. B8 (1973) 2965
38. V. Saile, W. Steinmann and E.E. Koch, in Extended Abstracts, Fifth International Conference on VUV Radiation Physics, Vol. 1, eds. M.C. Castex, M. Pouey and N. Pouey, publ. "V.U.V.5", C.N.R.S. Meudon, 1977, p. 199
39. U. Rössler, Phys. Stat. Sol. 42 (1970) 345
40. A.B. Kunz and D.J. Mickish, Phys. Rev. B8 (1973) 779

Density n (10^{22}cm^{-3})	E_{pc}^i (eV)	v_o (eV)	E_{Th}^i (eV)	P_+^i (eV)	E_2^i (eV)	B^i (eV)	ΔE_c (eV)	Δ_1 (eV)	m^* exptl.	m^* calc.
1.66	10.95	-0.26 ^(b)	11.21 ^(d)	-0.91 ^(g)	9.98 ^(h)	3.88 ^(j)	-1.6 ⁽ⁿ⁾	1.07 ^(h)	0.55 ^(o)	0.81 ^(s)
1.98	10.94	-0.22 ^(b)	11.15 ^(d)	-0.97 ^(g)	10.03 ^(h)	3.62 ^(j)	-1.4 ⁽ⁿ⁾	1.00 ^(h)	0.56 ^(o)	0.78 ^(s)
2.11	10.94	-0.17 ^(b)	11.11 ^(d)	-1.02 ^(g)	10.14 ^(h)	3.20 ^(j)	-1.1 ⁽ⁿ⁾	0.96 ^(h)	0.54 ^(o)	0.75 ^(s) 0.18 ^(t)
Solid	10.97	0.3 ^(c)	10.7 ^(d)	-1.4 ^(g)		2.36 ^(k)			0.47 ^(p)	0.45 ^(u)
	10.6 ^(a)		10.2 ^(e)		9.97 ^(a)	4.00 ^(l)	-2.25 ^(l)	1.31 ^(a)	0.80 ^(g)	0.44 ^(v)
			10.4 ^(f)		10.53 ⁽ⁱ⁾	1.76 ^(m)	0.0 ^(m)	0.75 ^(m)	0.35 ^(r)	

Table 1 Exciton parameters in Xe/Ar at three fluid densities and in the solid.
For the notation see text.

- (a) Ref. 2,
- (b) Ref. 26,
- (c) Ref. 37, pure Ar,
- (d) $E_{pc}^i + v_o$,
- (e) Ref. 8,
- (f) Ref. 9,
- (g) calculated from Eq. 1, see text,
- (h) Ref. 13,
- (i) re-assigned data of Ref. 2,
- (j) from E_2^i and E_{pc}^i , see text,
- (k) Ref. 38,
- (l) based on E_{pc}^i and Ref. 2,
- (m) based on E_{pc}^i and re-assigned data of Ref. 2,
- (n) from E_1^i exp from Ref. 13 and B^i ,
- (o) from B^i and ϵ , see text,
- (p) from B^i of Ref. 38 and ϵ ,
- (q) using B^i based on E_{pc}^i and Ref. 2 as well as ϵ ,
- (r) using B^i based on E_{pc}^i and re-assigned data of Ref. 2 as well as ϵ ,
- (s) Ref. 35, pure argon,
- (t) Ref. 42, based on photodetachment from O_2^- in argon,
- (u) Ref. 39, pure argon,
- (v) Ref. 40, pure argon.

Figure Captions

Figure 1 Photoconductivity excitation spectra of fluid argon doped by 1.6 ppm xenon at different fluid densities: a - 1.09×10^{22} , b - 1.76×10^{22} , c - $2.03 \times 10^{22} \text{ cm}^{-3}$; d - solid

Figure 2 The photoconductivity threshold of Xe/Ar as a function of the density of the host. Xenon concentrations: Δ - 1.6, \circ - 20, \bullet - 30 and $*$ - 220 ppm. \blacksquare is E_G^i from Ref. 1.

Figure 3 The adiabatic polarization energy P_+^i of a xenon impurity in fluid argon host as a function of fluid density. The meaning of the symbols Δ , \circ , \bullet and $*$ as for Fig. 2. ∇ and ∇ are obtained from E_{pc}^i from this work and taking V_0 from Ref. 37 and Ref. 41 respectively. $-\cdot-\cdot-$ P_+^i calculated from Eq. 2. $----$ from Ref. 32.

Figure 4 Photoconductivity excitation spectra of fluid argon doped by 30 ppm xenon, at different fluid densities: a - 0.88×10^{22} , b - 1.36×10^{22} and c - $1.8 \times 10^{22} \text{ cm}^{-3}$.

Figure 5 Perturbed atomic levels and excitons as a function of density.
 \bullet photon energies of the photocurrent minima. The other points are absorption peaks from Ref. 13: Δ - $6s[0\ 1/2]_1^0$ and $n'=1$; \triangle - $n=2$; \square - $5d[0\ 1/2]_1^0$; ∇ - $5d[2\ 1/2]_3^0$, \blacklozenge - $5d[1\ 1/2]_1^0$; \blacksquare - $7s[1\ 1/2]_1^0$.

Figure 6 Photoconductivity excitation spectra of fluid krypton doped by 10 ppm xenon at different fluid densities: a - 1.34×10^{22} ; b - 1.60×10^{22} ; c - $1.77 \times 10^{22} \text{ cm}^{-3}$.

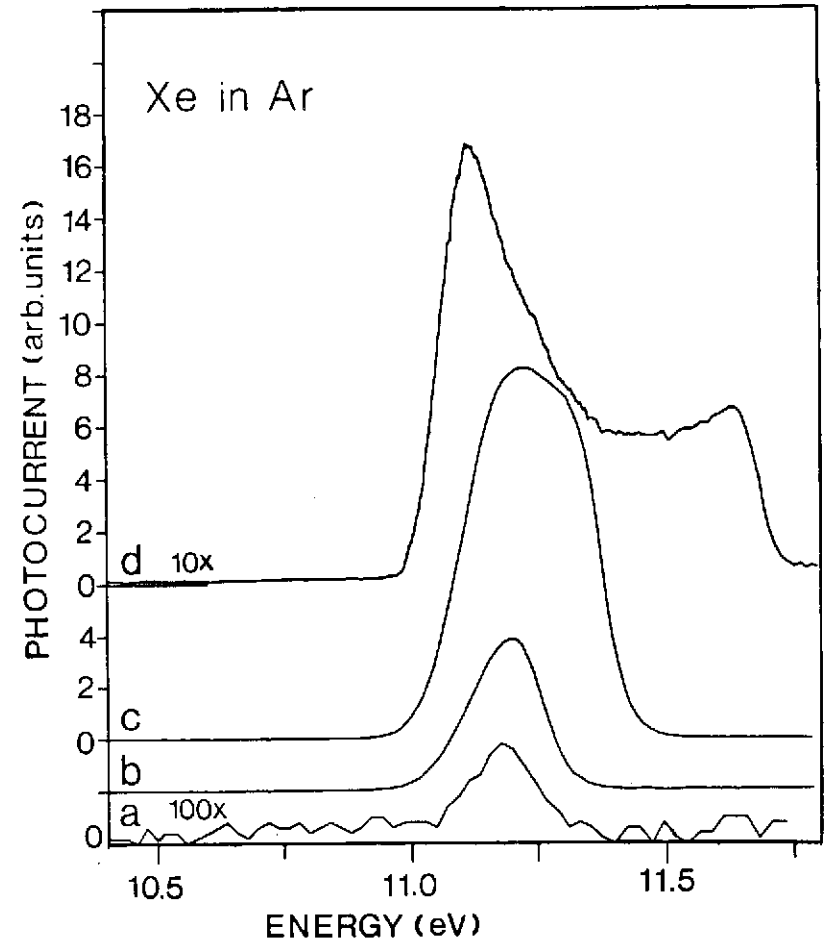


Fig. 1

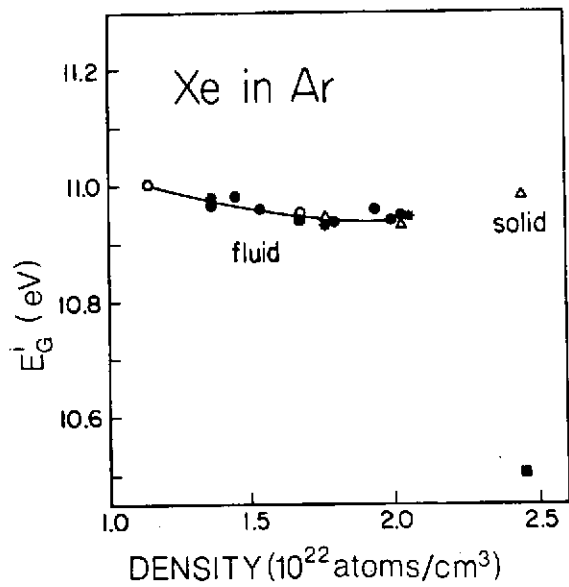


Fig. 2

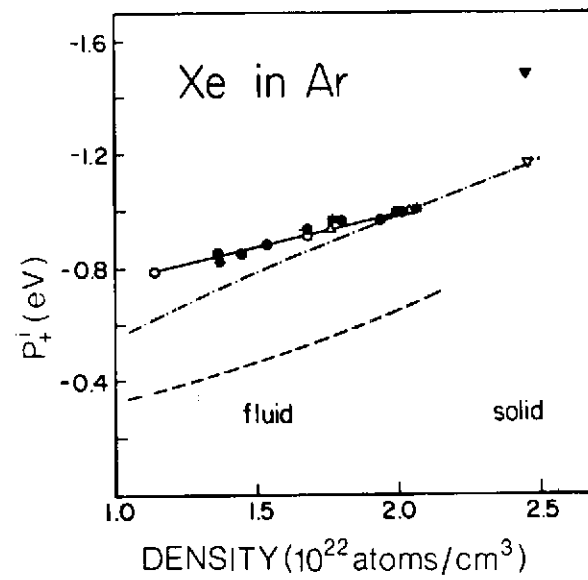


Fig. 3

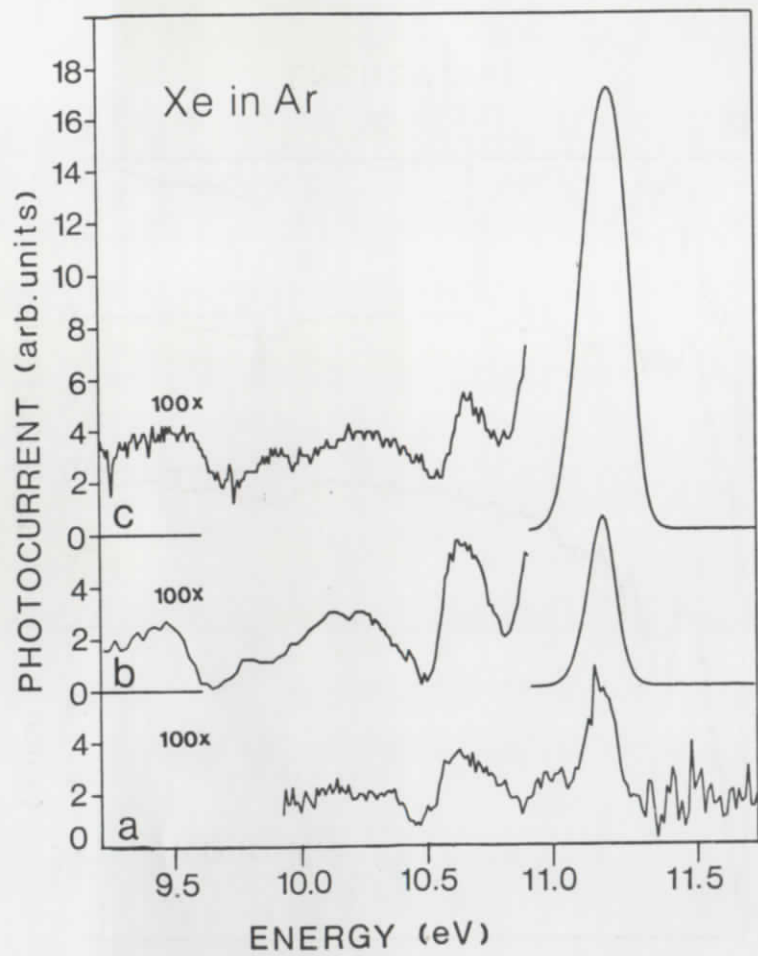


Fig. 4

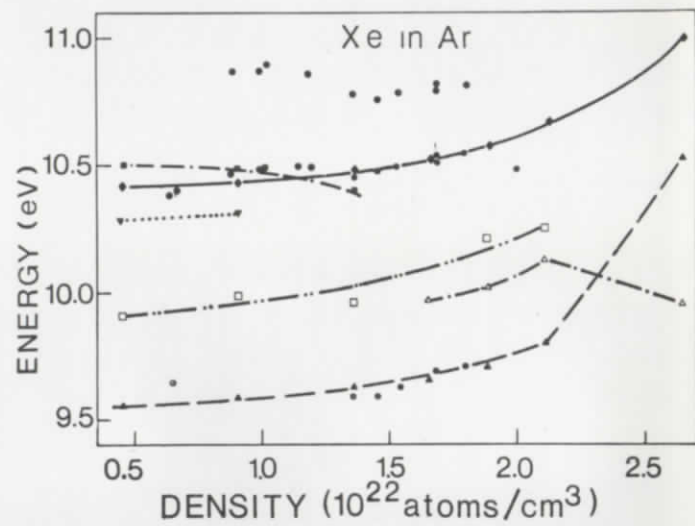


Fig. 5

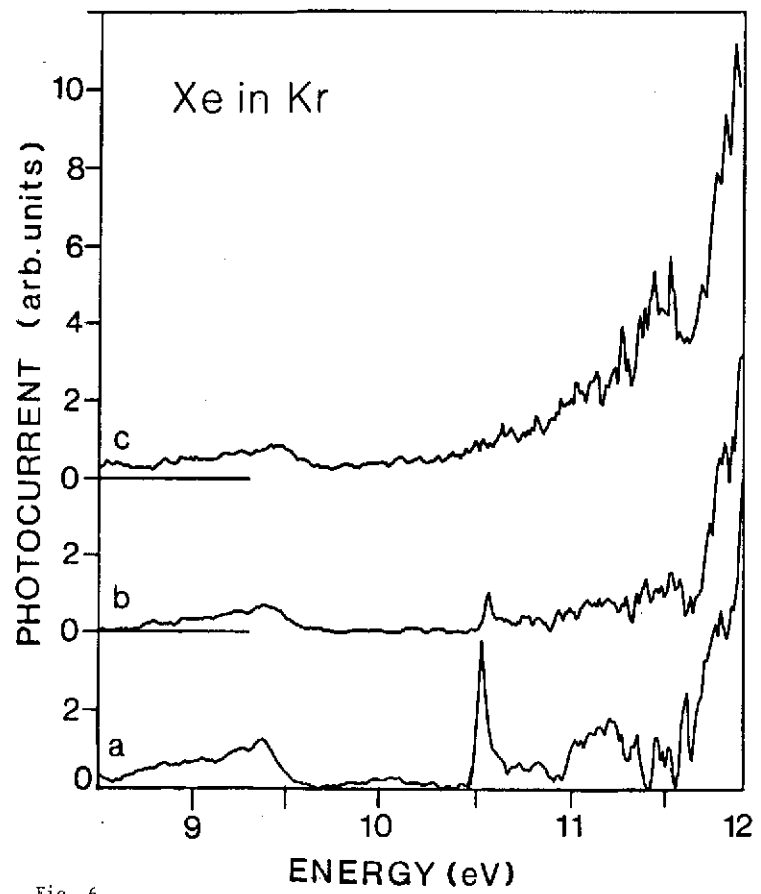


Fig. 6